Research Applications of Positron Emission Tomography/Magnetic Resonance (PET/MR) Imaging in Brain Tumors

Shuangshuang Song, Kun Guo, Zhilian Zhao, Zhigang Qi, and Jie Lu

In recent years, the incidence rate of brain tumors, for which surgical resection is the preferred treatment, has increased, and it is currently approximately 8.3–11 per 100,000 individuals. Gliomas are the most common type of primary intracranial tumors; they account for approximately 30% of all central nervous system (CNS) tumors and 70% of all primary brain tumors in adults and can be divided according to the World Health Organization (WHO) classification into low (WHO grades I and II) and high grades (WHO grades III and IV). Patients with gliomas tend to have a poor prognosis, although the prognosis is also dependent on the patient's age at onset, tumor location, surgical method, postoperative adjuvant therapy, and the molecular and genetic subtyping of the tumor(s). Low-grade gliomas typically have a more favorable prognosis than high-grade gliomas; therefore, the accurate preoperative classification of gliomas is of crucial significance to the formulation of treatment plans and prognostic prediction. There are significant limitations to using conventional MRI for the classification and diagnosis of gliomas, as this technique is based on characteristics such as contrast enhancement, space-occupying effects, edema, and necrosis. For instance, certain low-

grade gliomas may exhibit contrast enhancement, whereas certain high-grade gliomas may not. Primary central nervous system lymphoma (PCNSL) is a rare subtype of non-Hodgkin's lymphoma that is highly invasive but relatively sensitive to radiotherapy and chemotherapy. The incidence rate of PCNSL, which can affect the brain parenchyma, meninges, and spinal cord, has grown among the immunocompetent population in recent years, although it is more common in the immunocompromised population. Pathologically, the vast majority of cases are classified as large B-cell lymphoma. The average age at diagnosis for PCNSL is 60 years, and it is more prevalent among women. The age of onset of PCNSL among lymphoma patients with acquired immunodeficiency syndrome (AIDS) tends to be relatively younger.

Brain metastasis is another common feature of intracranial tumors among adults, occurring in 15–40% of cancer patients. Nevertheless, improvements in methods of diagnosis and treatment, as well as advancements in neuroimaging techniques, have led to a higher detection rate of brain metastases. Lung, breast, colorectal, and genitourinary cancers, as well as melanoma, are all prone to brain metastases, although the most common route of spread is via blood-borne metastasis, which is especially common within the territory of the middle cerebral artery. Upon initial diagnosis, approximately 50% of metastases are solitary, occurring in the cerebral hemi-

S. Song · K. Guo · Z. Zhao · Z. Qi · J. Lu (✉)
Department of Radiology and Nuclear Medicine,
Xuanwu Hospital, Capital Medical University,
Beijing, China

sphere (60%), cerebellar hemisphere (30%), and brainstem (10%). It is easier to diagnose patients with multiple metastases and a known history of tumors than diagnosing patients with an unknown history of tumors, upon the discovery of brain metastases, especially in cases of solitary brain metastases. In the latter case, therefore, a combination of imaging methods is required to achieve a correct diagnosis.

11.1 Research Applications of MRI in Brain Tumors

Since the advent of computed tomography (CT) and MRI, imaging has played an increasingly important role in guiding the surgical and radiotherapy treatment of brain tumors. Conventional MRI can be used to localize tumors, as well as display their morphology, boundaries, signal characteristics, and enhancement features. These conventional images are sufficient to aid in diagnosis or guide treatment; however, in some patients, a diagnosis cannot be confirmed based on conventional MRI alone, and additional information is needed for the differential diagnosis to facilitate more precise surgical planning. In other patients, it is necessary to observe the tumor-induced functional changes and determine the relationship between the tumor and functional brain areas, necessitating the use of more advanced functional MRI (fMRI) techniques. fMRI is a relatively recent imaging technology, which was developed in the 1990s. In a broad sense, fMRI includes diffusion-weighted imaging (DWI), perfusion-weighted imaging (PWI), diffusion tensor imaging (DTI), blood-oxygen-level-dependent (BOLD) imaging, magnetic resonance spectroscopy (MRS), and susceptibility-weighted imaging (SWI). These new MRI techniques have not only enhanced the accuracy of preoperative assessments and promoted the improvement of surgical procedures but have also provided excellent assistance to the formulation of radiotherapy and chemotherapy plans, and have become key tools in the evaluation of treatment prognosis.

## 11.1.1 Research Applications of DWI in Brain Tumors

DWI reflects the functional characteristics of tumors through the diffusion status of the tumor tissues. The DWI-derived quantitative indicator, the apparent diffusion coefficient (ADC), can describe the rate and range of the free diffusion of water molecules in different directions on the DWI map. It quantifies the diffusion of water molecules in tissues under the action of a diffusion gradient and is related to various factors, including the number, size, and arrangement of cells, extracellular space, nuclear-cytoplasmic ratio, and microcirculatory perfusion. Using ADC values, it is possible to predict the tumor classification and molecular subtype, determine the treatment response and evaluate the prognosis. DWI can also be utilized to quantitatively analyze the diffusion status of brain tumors.

The restricted diffusion characteristic of brain tumors is helpful for the qualitative diagnosis of brain tumors. Compared to normal brain parenchyma, tumorous lesions exhibit varying degrees of restricted diffusion due to increased cell density and reduced extracellular space. DWI can help to determine the tissue of origin for brain metastases as follows: In general, well-differentiated adenocarcinomas present hypointense DWI signals, whereas metastases from small- and large-cell neuroendocrine carcinomas present as hyperintense DWI signals. Furthermore, DWI can discriminate between brain tumors and abscesses, which is immensely helpful for the differential diagnosis of ring-enhancing tumors and abscesses. The ADC value within the cavity of a brain abscess is significantly reduced, whereas restricted diffusion is generally not observed within the intratumoral cavity, but at the tumor wall, of tumors with liquefactive necrosis. High-grade gliomas are characterized by rapid cell proliferation, increased cell density, smaller extracellular spaces, and an increase in the nuclear-cytoplasmic ratio, which can restrict the movement of water molecules, thereby increasing DWI signals and decreasing ADC values (Figs. 11.1 and 11.2). In contrast, low-grade gliomas have relatively high ADC
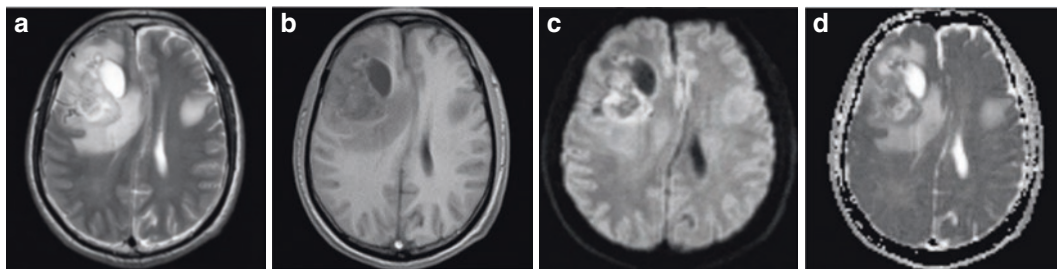
Fig. 11.1 IDH-wildtype glioblastoma, WHO grade IV. A 56-year-old male patient whose MRI shows an irregular, abnormal space-occupying lesion in the right frontal lobe, with significant signal heterogeneity and intralesional cystic changes and necrosis. The solid compartment of the tumor shows isointense and slightly hyperintense T_2WI signals (**a**); slightly hypointense T_1WI signals (**b**); hyperintense DWI signals (**c**); and hypointense ADC signals, signifying the restricted diffusion of the tumor parenchyma (**d**)
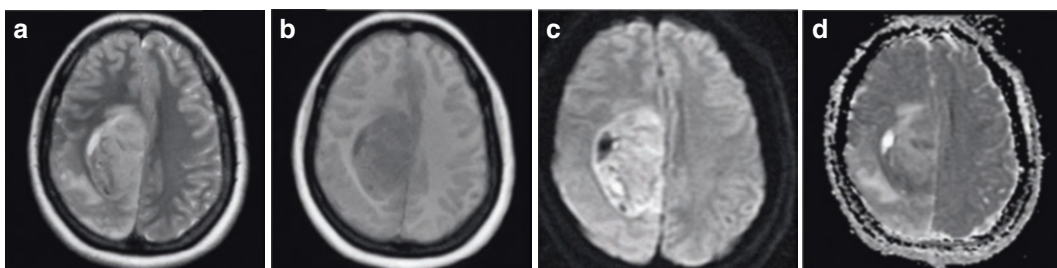
Fig. 11.2 IDH-mutant anaplastic oligodendroglioma, WHO grade III. A 46-year-old female patient whose MRI shows an oval space-occupying lesion in the right parietal lobe, with a lack of intralesional signal homogenei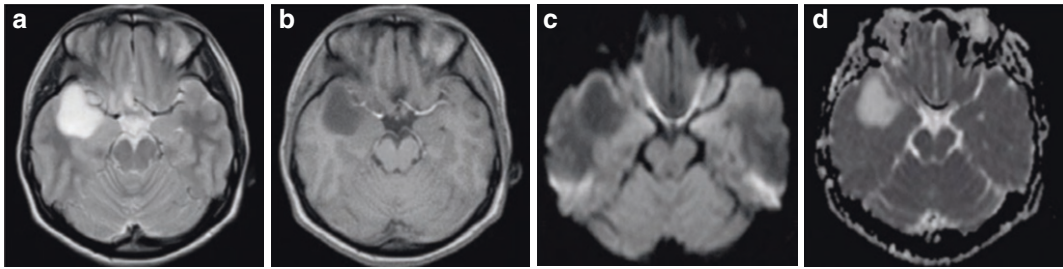ty. Transverse T_2WI shows isointense and slightly hyperintense signals (**a**); transverse T_1WI shows slightly hypointense signals (**b**); transverse DWI shows isointense and hyperintense signals (**c**); and transverse ADC shows hypointense and hyperintense signals, signifying the regional restricted diffusion of the tumor parenchyma (**d**)

values (Fig. 11.3); therefore, an ADC value of 1.185×10^{-3} mm^2/s can be used as a cutoff point to differentiate between low- and high-grade gliomas, with a sensitivity of 97.6% and specificity of 53.1%. A meta-analysis evaluating the use of ADC values to differentiate between the grades of glioma showed that preoperative ADC values had a relatively high accuracy for discriminating between low- and high-grade gliomas. The overall sensitivity and specificity were 0.85 and 0.80, respectively; the positive and negative likelihood ratios were 4.25 and 0.18, respectively, and the area under the receiver operating characteristic curve (AUC) was 0.90. Furthermore, quantitative ADC values showed high discriminatory accuracy for low- and high-grade gliomas.

In 2016, the molecular subtyping of gliomas was incorporated into the WHO classification of CNS tumors, based on histological subtyping. Isocitrate dehydrogenase (IDH) mutations were identified as key biomarkers, and gliomas were divided into IDH-mutant and IDH-wildtype gliomas. Studies have found that IDH-wildtype gliomas have lower ADC values (Fig. 11.1) than IDH-mutant gliomas (Figs. 11.2 and 11.3) and that the minimum ADC value (0.9×10^{-3} mm^2/s) shows the highest sensitivity (91%) and specificity (75%) for predicting IDH-wildtype gliomas. The relative mean ADC could predict IDH mutation status without being affected by the WHO grade of the tumor, and the optimal cut-off value for differentiating between IDH-mutant and wildtype gliomas was 1.2, with a sensitivity of 81.9%, specificity of 74.6%, and AUC of 0.790.

The manifestations of PCNSL in conventional imaging are diverse, which often leads to difficulties in differential diagnosis. DWI is a valuable technique for the diagnosis and differential diagnosis of PCNSL. Due to its high cell density, PCNSL is characterized by restricted diffusion,

Fig. 11.3 IDH-mutant oligodendroglioma, WHO grade II. A 26-year-old female patient whose MRI shows an abnormal circular lesion in the right temporal lobe with homogenous signal intensity. Transverse T_2WI shows hyperintense signals (**a**); transverse T_1WI shows hypointense signals (**b**); transverse DWI shows hypointense signals (**c**); and transverse ADC shows hyperintense signals, signifying the absence of restricted diffusion (**d**)
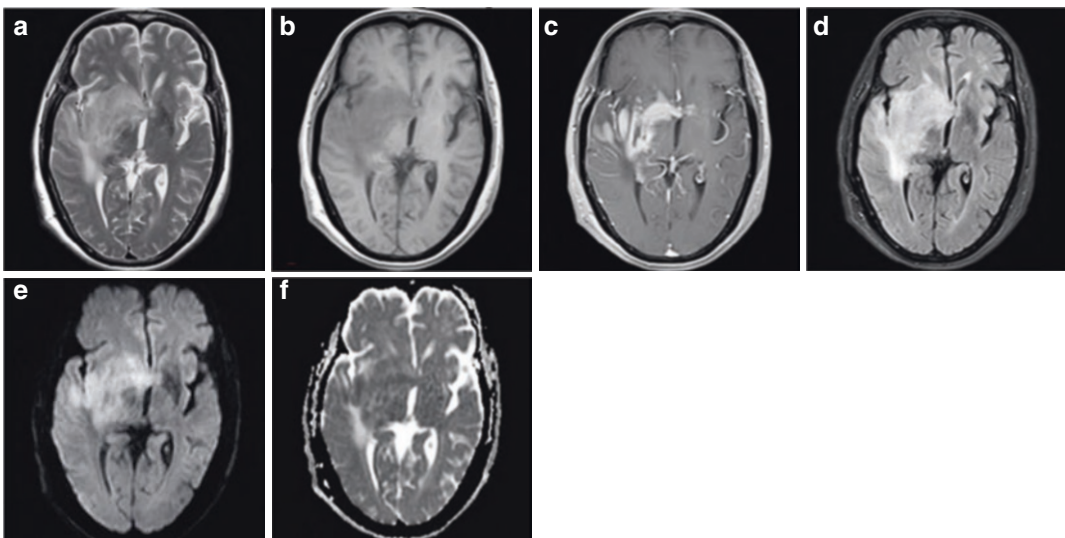
Fig. 11.4 Flaky space-occupying lesion of the right basal ganglia. T_2WI shows heterogeneous hyperintensity (**a**); T_1WI shows hypointensity (**b**); contrast-enhanced T_1WI shows homogenous enhancement (**c**); FLAIR shows heterogenous hyperintensity (**d**); DWI (b-value = 800) shows hyperintensity of the lesion in the right basal ganglia (**e**); and transverse ADC value shows heterogeneous decrease, signifying restricted diffusion (**f**)

which presents as hyperintense signals on DWI maps with decreased ADC values (Fig. 11.4). Although glioblastomas and metastases can also exhibit restricted diffusion, PCNSL tends to have lower ADC values. Additionally, ADC values can aid in the prediction of prognosis, as previous studies have shown that PCNSL patients with lower ADC values in the tumor enhancement area before treatment had shorter survival times. Furthermore, ADC values can also be used to determine treatment response, as repeat testing of ADC values in patients with PCNSL after different chemotherapy regimens allows the monitoring of significant changes in ADC values, which were found to be significantly associated with patient survival. In fact, one study showed that lymphoma patients whose minimum ADC value before treatment was $<384 \times 10^{-6}$ mm^2/s had faster disease progression and poorer prognosis.

11.1.2 Research Applications of DTI in Brain Tumors

DTI, a more recent imaging technique based on DWI, can be used to accurately display the direction and quantification of the diffusion motion exhibited by the water molecules in lesions.

When applied to the diagnosis of brain tumors, physicians can utilize DTI to measure fractional anisotropy (FA) and ADC values, to determine the diffusion direction of the water molecules in brain tissues, while also determining the integrity of the nerve fiber structures and the relationship of white matter fiber bundles with tumors, thereby facilitating more precise surgical planning. Holodny et al. used DTI to determine the positional relationship between corticospinal tracts and adjacent brain tumors, which helped delineate the extent of surgical resection. Three different types of relationship were identified between infiltrative brain tumors and neighboring corticospinal tracts: (1) the corticospinal tract was unaffected by the tumor; (2) the tumor was adjacent to the corticospinal tract, and involvement was suspected; and (3) the tumor had infiltrated the corticospinal tract, leading to the breakage, displacement, and deformation of adjacent white matter tracts. In a randomized prospective study, Wu et al. performed preoperative DTI on patients with gliomas and found that a more involved surgical resection in patients with corticospinal tract involvement ensured an increased preservation of postoperative nerve function, as well as a longer survival time compared to patients who did not undergo a preoperative evaluation. Chen et al. utilized DTI to track the white matter fibers in the peritumoral edema zone of glioma patients and found that the degree of fiber bundle destruction directly reflected the extent of tumor cell infiltration, helping to confirm the boundary of the tumor infiltration zone. In another study, DTI was used to reconstruct white matter fiber bundles dominated by the effective fibers of pyramidal tracts, to ensure the maximum surgical resection of tumors and the preservation of the effective fibers of pyramidal tracts. The results of that study indicated that the disability rate 3 months after surgery was significantly lower in these patients than in those who underwent conventional total tumor resections. Therefore, the DTI-guided resection of gliomas involving crucial nerve fiber bundles not only assists surgeons in ensuring maximum tumor resection but can also reduce the postoperative disability rate, improving the patient's postoperative quality of life.

11.1.3 Research Applications of PWI in Brain Tumors

The methods of perfusion MRI currently utilized to evaluate the hemodynamic changes of brain tumors primarily include dynamic susceptibility contrast (DSC)-PWI, dynamic contrast-enhanced (DCE)-MRI, and arterial spin labeling (ASL). Both DSC-PWI and DCE-MRI require the injection of a contrast agent, and by detecting the signal changes induced by the bolus of contrast agent, these techniques can be used to acquire signal intensity-time curves, which can be converted to tissue contrast agent concentration-time curves, and regional hemodynamic parameters can be calculated by fitting different mathematical models. Commonly used parameters in DSC-PWI include relative cerebral blood volume (rCBV), regional cerebral blood flow (rCBF), mean transit time (MTT), and time to peak (TTP). Of these, rCBV is the most commonly utilized parameter in the assessment of brain tumors. Commonly used parameters in DCE-MRI include the plasma-to-extravascular volume transfer (K^{trans}), fractional volume of the extravascular extracellular space (V_e), fractional plasma volume (V_p), and extravascular-to-plasma volume transfer (K_{ep}), of which, K^{trans} is most commonly utilized. Due to the complexities of quantifying DCE parameters, the clinical applications of this technique are limited. ASL does not require the injection of contrast agents, but instead uses the hydrogen protons of arterial blood as an endogenous tracer to acquire information on the perfusion of brain tissues, and accurately assess tumor angiogenesis in a non-invasive manner.

Early studies have shown that elevated rCBV is associated with more active angiogenesis and aggressiveness of malignant tumors; therefore, rCBV is a potential imaging biomarker for preoperative tumor grading. Furthermore, significant differences have been found between the rCBV values of high- and low-grade brain tumors, with high-grade gliomas (WHO grades III and IV) having higher rCBV values than low-grade gliomas (WHO grades I and II). However, there is currently no unified standard for rCBV cut-off values for the classification of high- and low-

grade gliomas. Some studies have defined rCBV-$_{max}$ = 1.7 as the cut-off value to differentiate between the two, whereas others have recommended a cut-off value of rCBV$_{max}$ = 2.01. Additionally, brain tumors of different pathological types also present different perfusion manifestations. For example, even though oligodendrogliomas are low-grade tumors, they tend to exhibit relatively high rCBV, which may be due to the abundant blood vessels and dense capillary networks present in the tumors. In addition to exhibiting restricted diffusion, CNS lymphomas are characterized by distinct perfusion imaging features. In conventional contrast-enhanced MRI, lymphomas are significantly enhanced, with findings similar to those of glioblastomas, brain abscesses, and demyelinating lesions, which may cause difficulties in the differential diagnosis. Perfusion imaging shows that lymphomas are hypoperfused compared to glioblastomas and other lesions, which is a helpful imaging feature for differential diagnosis.

Perfusion imaging can also help to determine the molecular characteristics of gliomas. Many studies have found that compared with IDH-wildtype (Fig. 11.5), IDH-mutant gliomas have lower rCBV values (Fig. 11.6), while all IDH-wildtype gliomas, regardless of the histological grade, show significantly elevated perfusion. This may be related to the more active angiogenesis and less heterogenous microenvironment of IDH-wildtype gliomas. rCBV can serve as a robust, non-invasive imaging biomarker for predicting IDH mutation status. Additionally, DSC-PWI can be performed to discriminate the treatment responses of gliomas, especially between tumor pseudo-progression and tumor recurrence, which is an issue of significant clinical concern. More specifically, tumor pseudo-progression exhibits a lower level of perfusion than tumor recurrence, which may be attributed to the decreased cell density and vascularization of pseudo-progressive lesions, as opposed to the neovascularization that frequently occurs in tumor recurrence, resulting in increased intralesional blood supply and elevated rCBV. Furthermore, both the rCBV value of DSC-PWI and the K^{trans} of DCE have good discriminant abilities for radiation necrosis and tumor recurrence. One study using 1.23 as the rCBV cut-off value found that the sensitivity of discriminating between the two was 88% and specificity was 75%; whereas adopting a K^{trans} cut-off value of 28.76 gave a sensitivity of 89% and specificity of 97%.

Owing to its convenience and speed, ASL perfusion imaging also plays a vital role in the preoperative classification, treatment follow-up, and differential diagnosis of gliomas. High-grade gliomas exhibit significantly higher rCBF than low-grade gliomas (Fig. 11.7). However, one study demonstrated that ASL imaging could not differentiate between WHO grade III and IV gliomas, because WHO grade III gliomas are pri-
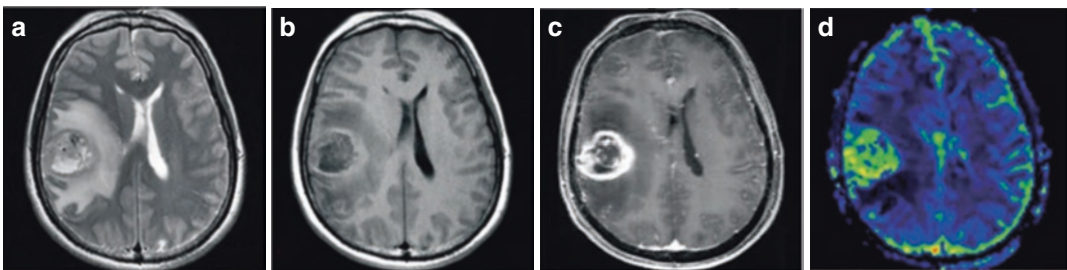
Fig. 11.5 IDH-wildtype glioblastoma, WHO grade IV. A 53-year-old male patient whose MRI shows a circular mass in the right parietal lobe. Transverse T$_2$WI shows heterogenous mixed hyper- and hypointense signals (**a**); transverse T$_1$WI shows heterogenous iso- to hypointense signals (**b**), surrounded by finger-like edema; contrast-enhanced scan shows significant heterogenous ring-like enhancement (**c**); and the solid component of the lesion shows significantly elevated CBV, with relative mean CBV and relative maximum CBV of 2.78 and 6.63, respectively (**d**)
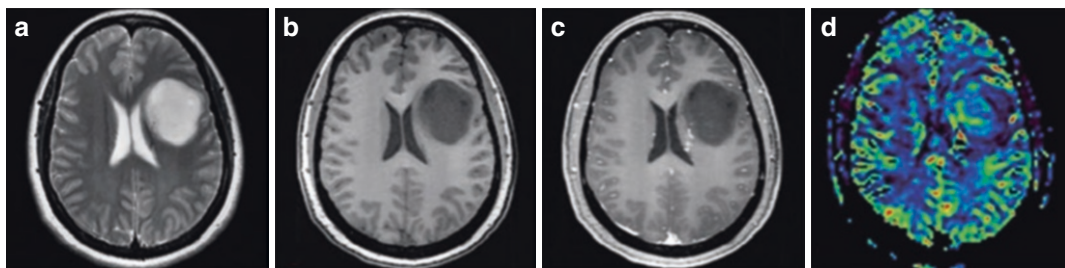
Fig. 11.6 IDH-mutant astrocytoma. A 31-year-old female patient whose MRI shows a circular mass in the left frontoparietal lobe. Transverse T_2WI shows heterogenous hyperintense signals (**a**); transverse T_1WI shows homogeneous hypointense signals (**b**), without no obvious signs of edema around the lesion; contrast-enhanced scan shows no significant enhancement (**c**); and the lesion shows slightly elevated CBV, with relative mean CBV and relative maximum CBV of 0.83 and 3.24, respectively, which were both lower than those of IDH wild-type glioma (**d**)
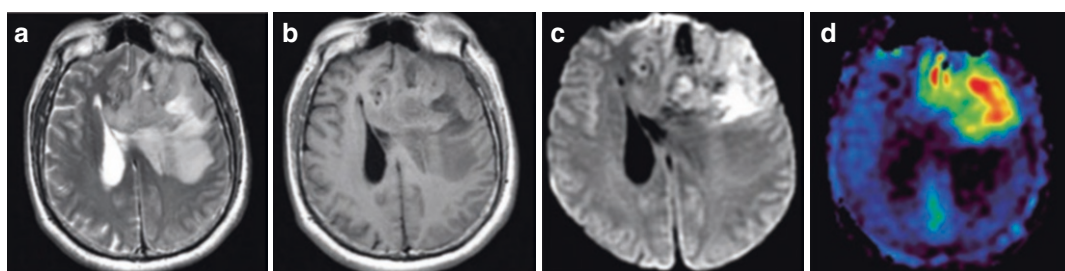
Fig. 11.7 IDH-mutant and 1p/19q co-deleted oligodendroglioma. A 48-year-old male patient whose MRI shows an irregular mass in the left frontotemporal lobe. Transverse T_2WI show heterogeneous hyperintense signals (**a**); transverse T_1WI shows homogeneous iso- to hypointense signals (**b**); transverse DWI shows mixed hyper- and hypointense signals (**c**); and lesion CBF is significantly higher than the contralateral side (**d**)

marily oligodendrogliomas with hyperperfusion, whereas WHO grade IV gliomas are primarily glioblastomas that may exhibit a variety of perfusion changes due to intratumoral cystic necrosis. Additionally, ASL can help differentiate post-treatment responses in high-grade gliomas. One key point in the evaluation of glioblastomas following chemotherapy and radiotherapy is to determine whether the MRI T_1-enhanced region is tumor recurrence or tumor pseudo-progression. Studies have found a significant difference in rCBF between the two, with postoperative brain tumor recurrence showing a significantly higher rCBF than tumor pseudo-progression, clearly differentiating between the two conditions. Another study found that ASL can be used to rapidly and easily differentiate between PCNSL and glioblastoma, as PCNSL shows a significantly lower CBF than glioblastoma, while the AUC value for the differential diagnosis between the two is >0.9.

11.1.4 Research Applications of Proton MRS in Brain Tumors

MRS can provide information on various metabolites in brain tumors, which can facilitate the differential diagnosis while also providing valuable information for the biopsy localization, grading, treatment evaluation, and prognostic determination of brain tumors. MRS is divided into single- and multi-voxel spectroscopy. Single-voxel spectroscopy is easy to operate and suitable for clinical applications, whereas multi-voxel spectroscopy can evaluate the spatial distribution

of metabolites within a lesion in one scan session, which is helpful for assessing the extent and malignancy of the lesion, formulating treatment plans, and determining the site of biopsy.

Different types and grades of brain tumors exhibit different MRS findings. For most brain tumors, MRS reveals an increased choline (Cho) peak, decreased N-acetylaspartate (NAA) peak, and increased Cho/creatine (Cr) and Cho/NAA ratios. The increase in Cho peak is associated with increased tumor cell density and accelerated cell membrane Cho metabolism, whereas the decrease in NAA peak is associated with reduced neuronal function and damaged neuronal structure in the tumor area. Generally speaking, the Cr peak remains relatively unchanged in low-grade gliomas, but shows a decrease in high-grade gliomas. Nevertheless, despite the frequent occurrence of increased Cho/Cr and Cho/NAA in high-grade gliomas, there are overlaps in MRS findings among different grades of tumors. The lactate (Lac) and lipid (Lip) peaks cannot be observed in normal brain tissues, and are found only in tumor tissues, especially high-grade tumors. The Lac peak can be seen across all grades of gliomas, whereas the combination of the Lac and Lip peaks allows the discrimination of high-grade (Fig. 11.8) from low-grade gliomas (Fig. 11.9).

The MRS findings of PCNSL also involve elevated Cho/Cr and Cho/NAA ratios, but studies have found that more than 90% of cases exhibited Lac and Lip peaks, which were not proportional to the degree of intralesional necrosis. This feature may help to distinguish PCNSL from glioblastoma. MRS can also be applied to discriminate brain tumors from non-neoplastic lesions; however, relying on MRS alone can often lead to difficulties in differential diagnosis. For example, demyelinating lesions can exhibit increased Cho/Cr and decreased NAA/Cr, which are similar to the MRS findings of tumors. Therefore, the combination of conventional MR findings with clinical presentations is critical for similar lesions. A meta-analysis showed that MRS can also be utilized to differentiate high-grade gliomas that are
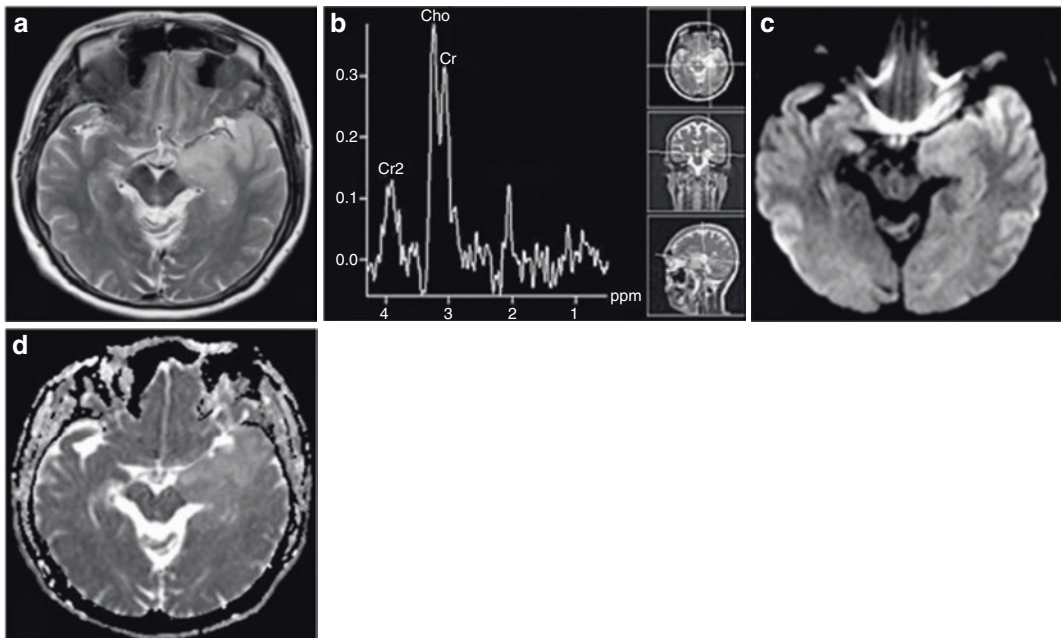
Fig. 11.8 Left temporal lobe glioma, WHO grade II. MRI shows glioma of the left temporal lobe, with hyperintense signals observed in transverse T2WI (**a**). Multivoxel MRS shows elevated Cho/Cr and reduced NAA/Cr (**b**). Transverse DWI (b-value = 800) shows mixed signals in the left temporal lobe mass, dominated by iso- to hyperintense signals (**c**), whereas no significant decrease was observed in ADC value (**d**)
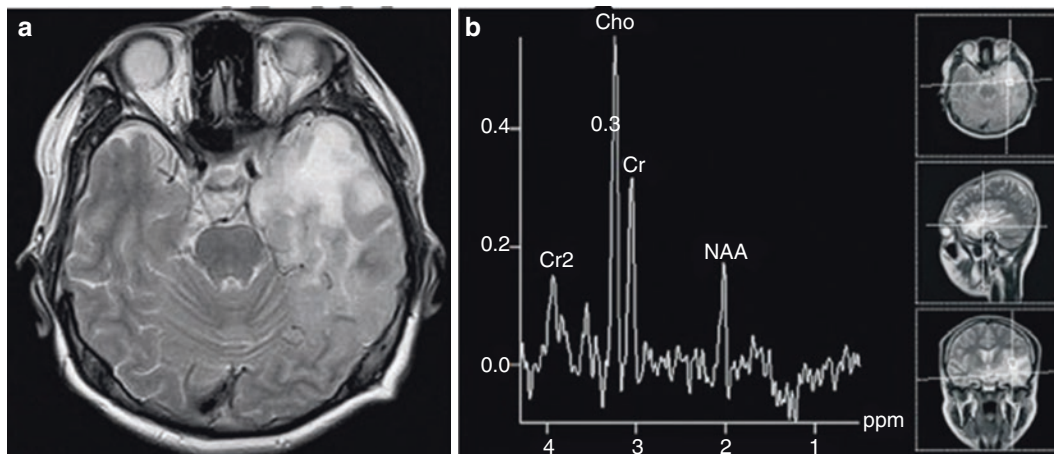
Fig. 11.9 Left temporal lobe glioma, WHO grade III. Transverse T_2WI shows hyperintense signals in the left temporal lobe (**a**); multi-voxel proton MRS shows increased Cho/Cr, decreased NAA/Cr, and an inverted Lac peak at 1.33 ppm (**b**)

treatment-responsive from true tumor progression, attaining a sensitivity of up to 91% and specificity of 95% in the differential diagnosis between the two. Among all indicators, the Cho/Cr ratio showed the greatest significance in differential diagnosis.

11.1.5 Research Applications of SWI in Brain Tumors

At present, SWI is not routinely performed as part of head MRI sequences. Information on the morphology and distribution of hemorrhage and calcification in gliomas is very valuable for the diagnosis and differential diagnosis of such tumors. However, the display of intratumoral calcification and microbleeds is difficult to achieve using conventional spin-echo (SE) sequences (i.e., T_1WI and T_2WI), but this can be easily accomplished using SWI, which can also produce phase images to differentiate between calcification and hemorrhage. Therefore, SWI is a useful tool for the non-invasive evaluation of CNS gliomas. SWI can increase the detection rate of intratumoral hemorrhage in the brain, which has significant implications for the quantitative diagnosis of tumors and guidance of clinical surgery. Furthermore, since SWI mainly relies on the magnetic susceptibility differences among tumor tissues to form image contrast, it can more clearly display tumor boundaries. As for the qualitative aspects of brain tumors, SWI can provide useful information for qualitative diagnosis with respect to vascular proliferation and microbleeds. Early manifestations of basal ganglia germinoma include patchy lesions in the basal ganglia without space-occupying effects, accompanied by atrophy of the ipsilateral sulci and midbrain, which can easily be confused with cerebral infarction. SWI can aid in the identification of neovascularization within germinomas, facilitating early diagnosis. Solitary-enhancing nodules in the brain may be solitary granulomas, demyelinating pseudotumor, lymphomas or glioblastomas. These lesions may sometimes be difficult to differentiate, and SWI can provide valuable information for their differential diagnosis. Studies have shown almost all glioblastomas exhibit hypointense SWI signals representing blood metabolites, calcifications, and veins, whereas these signals are rarely observed in non-neoplastic lesions and lymphomas. Therefore, this sign can be exploited for differential diagnosis, attaining a specificity of nearly 100% for discrimination.

Invasive brain tumors tend to exhibit rapid intratumoral vascular growth and multiple micro-

bleeds. During the course of brain glioma growth, the increased secretion of vascular endothelial growth factor (VEGF) promotes the growth of immature new microvessels and increases microvascular density. Therefore, the detection of such intratumoral alterations facilitates the qualitative diagnosis of brain tumors. Furthermore, microvascular density is positively correlated with the pathological grade of gliomas. Therefore, the presence of SWI hypointensities, the proportion of the entire tumor occupied by hypointensities, and the morphology of hypointensities can also assist with the preoperative classification and evaluation of brain tumors. Researchers have observed that tumor classification based on SWI showed good concordance with T_1 enhancement. Mittal et al. found that brain tumors with higher PWI-derived rCBV values and MRS-derived Cho/Cr ratios showed more hypointensities on SWI. Additionally, the presence of intratumoral calcification, as well as the morphology and level of calcification, are important features in the evaluation of brain tumors, while SWI can display the calcified components of brain tumors. When detecting calcification in brain tumors such as oligodendrogliomas, the addition of SWI sequences led to a statistically significant increase in sensitivity (from 33 to 86%) but did not affect the specificity. SWI was also helpful in discriminating vestibular schwannomas from cerebellopontine angle meningiomas, as microbleeds can be observed in schwannomas but not meningiomas.

11.1.6 Research Applications of fMRI in Brain Tumors

The principle of craniocerebral tumor resection is the safe and maximal removal of tumors, while its challenge lies in grasping the balance between complete tumor resection and the preservation of function. However, functional localization is difficult due to a variety of factors, including individual differences in brain functional areas, the compression and displacement of functional areas by lesions, and the remodeling of functional areas. Therefore, it is extremely unreliable

to depend solely on the surgeon's subjective judgment to achieve the localization and protection of functional areas, while the objective and accurate localization of brain functional areas has now become a key technique that can determine the success of brain tumor surgery in functional areas. The most common imaging method currently used in the localization of brain functional areas is fMRI. By performing task-based fMRI research on patients with brain tumors, it is possible to identify and confirm the functional areas of language with a sensitivity and specificity of up to 90%. On top of this, task-based fMRI is also convenient and non-invasive, which has enabled this technique to play a crucial role in the intraoperative localization of cortical language areas in brain tumor surgery. Additionally, fMRI has shown a similar performance to invasive techniques in displaying motor networks or motor areas, and can therefore also serve as a simple and effective method for the preoperative evaluation of motor areas. Preoperative task-based fMRI has shown a relatively good performance in localizing the motor and supplementary motor areas; therefore, it is frequently integrated into neuronavigation systems to assess the spatial positional relationship of brain tumors with adjacent functional areas, in order to guide surgical resection (Fig. 11.10).

During the surgical process, factors such as the opening of the skull, loss of cerebrospinal fluid, and traction often lead to "shifts" in the actual intraoperative position of lesions. In most craniotomies, shifts of up to or even exceeding 1 cm can occur in brain tissues, which substantially reduces the accuracy of surgical procedures. However, since the advent of intraoperative MRI (iMRI), the real-time MRI-based acquisition of brain deformation and shift errors during the surgical process has become a reality, leading to significant improvements in the precision of navigation and localization. Many studies have shown that the application of iMRI can significantly increase the tumor resection rate and postoperative survival rate of patients, while its long-term clinical efficacy has also been verified. Additionally, the application of intraoperative fMRI in brain tumor surgery can also assist neu-
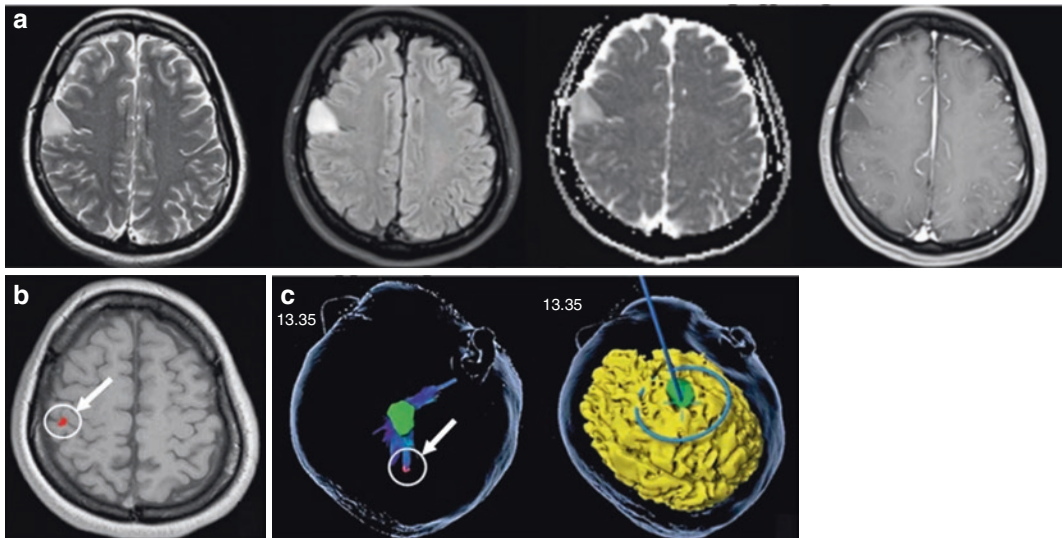
Fig. 11.10 Right frontal lobe oligodendroglioma, WHO grade II. A 27-year-old female patient, in whom a space-occupying lesion was discovered in the right frontal lobe 3 months ago. Patient's preoperative MRI, which revealed that the lesion was adjacent to the motor areas (**a**). Patient's preoperative fMRI motor activation map during hand movements (**b**). The tumor boundary and functional activation map were integrated into 3D navigation to assist in the avoidance of motor activation areas during surgery (**c**). Arrow: motor activation area

rosurgeons with avoiding cortical functional areas, thereby achieving precise resection. Wu et al. implemented intraoperative fMRI in the resection of patients with gliomas in the Broca area. In their study, patients underwent intraoperative awakening to perform language tasks in an awake state under anesthesia, which were combined with the simultaneous acquisition of fMRI information, in order to collect real-time activation information of the patient's cortical language areas during the operation. This approach not only enabled maximal tumor resection but also ensured the preservation of the patient's language function.

With the advancements in modern neurosurgery, the gradual deepening of our understanding on brain tumors is closely related to progress in neuroimaging. An increasing number of neurosurgeons are now implementing advance preoperative neuroimaging methods to facilitate surgical planning. Most fMRI techniques have good reproducibility, do not involve ionizing radiation, and incur relatively low costs; therefore, these techniques have significant implications for brain tumors with respect to surgical

planning, prognosis prediction, reduction of surgery-induced functional impairments and postoperative complications, improvement of postoperative quality of life, and promotion of further rehabilitation in postoperative neural function.

11.2   Research Applications of PET Imaging in Brain Tumors

With the rapid development of imaging techniques, the use of PET imaging has gradually become more widespread for the clinical diagnosis and treatment of brain tumors, demonstrating unique advantages in displaying the overall expression of tumor markers. PET imaging is now a new method for analyzing the molecular pathological characteristics of tumors and screening for targeted drugs. This technique allows the direct visualization of tumor biological processes at the molecular and cellular levels and enables the direct measurement of sugar, protein, lipid, and nucleotide metabolism; it is extensively applied in the diagnosis, classification, and effi-

cacy evaluation of brain tumors. Different PET imaging agents can reflect different characteristics in tumor cells.

11.2.1 Common PET Imaging Agents

11.2.1.1 Glucose Metabolism

Fluorodeoxyglucose (FDG) is currently the most frequently used PET imaging agent that reflects glycolysis in tissues and cells. The pathological basis of ^{18}F-FDG PET is that the cells of malignant tumors exhibit a higher uptake and utilization of glucose than those of normal tissues. The majority of brain tumors are characterized by glucose hypermetabolism, while the level of ^{18}F-FDG uptake is associated with the level of tumor malignancy. More specifically, CNS tumors with relatively low malignancy show a similar level of ^{18}F-FDG uptake to that of normal white matter, whereas tumors with relatively high malignancy tend to have elevated ^{18}F-FDG uptake, but which is often similar to that of gray matter.

11.2.1.2 Amino Acids and Choline

PET imaging agents for amino acid transport that are currently in common use include ^{11}C-methionine (^{11}C-MET), O-(2-[^{18}F]fluoroethyl)-L-tyrosine (^{18}F-FET), and ^{11}C-choline (^{11}C-CH). At present, ^{11}C-MET is the most established imaging agent for amino acids in clinical research, and its retention in gliomas mainly reflects the increase in amino acid transport activity, that is, the increase of protein synthesis in tumor cells. Under normal circumstances, brain tissues (except for the pituitary) tend to exhibit very low ^{11}C-MET uptake, implying that this compound can serve as an excellent imaging agent for brain tumors. ^{11}C-MET imaging is superior to ^{18}F-FDG imaging with respect to the diagnosis of gliomas, discrimination between tumor recurrence and necrosis, early evaluation of therapeutic efficacy, and the diagnosis of peritumoral tissues and low-grade gliomas. However, ^{11}C-MET has a relatively short half-life (about 20 min), which has restricted its application in clinical practice. ^{18}F-FET has a longer half-life (110 min) than

[11]C-MET, and its uptake does not depend on the disruption of the blood-brain barrier; therefore, it is more widely accepted in clinical applications. ^{18}F-FET PET imaging can facilitate the discrimination between brain tumors and non-neoplastic lesions, showing high sensitivity and specificity for the diagnosis of primary intracranial tumors. Furthermore, the time-activity curve acquired using dynamic ^{18}F-FET PET imaging can aid the classification and diagnosis of gliomas. This is because high-grade gliomas reach an early peak of ^{18}F-FET uptake at 10–15 min after injection, which is followed by a decrease, whereas low-grade gliomas tend to exhibit a delayed peak of ^{18}F-FET uptake that continues to rise steadily thereafter. In meta-analysis of 23 studies involving 994 patients, ^{18}F-FET PET showed a significantly higher sensitivity than ^{18}F-FDG PET for the preoperative classification of gliomas (88 vs 63%), as well as a higher specificity (89 vs 57%). In 2016, new content on molecular subtypes was added to the WHO classification of CNS tumors, which stipulated that histological morphology, WHO grade, and biomarkers must be combined in order to form an integrated diagnosis of gliomas. The most important among the molecular features are IDH mutation and chromosomal 1p/19q co-deletion status, which are intimately linked with the molecular subtyping of gliomas, formulation of individualized treatment plans, and efficacy of postoperative chemotherapy and radiotherapy. ^{18}F-FET PET imaging is useful for the prediction of glioma genotype, while also contributing clinically to prognostic prediction and the discrimination of metastasis from recurrence following radiosurgery. ^{11}C-CH is currently the most commonly applied imaging agent for Cho that can reflect its metabolism in tumors. ^{11}C-CH imaging can obtain a higher tumor-to-peripheral tissue uptake ratio than ^{11}C-MET imaging, producing better-quality images. However, ^{11}C-CH is also a non-specific tumor imaging agent, which may give rise to false positives and false negatives in tumor tests. For example, tuberculous meningiomas are positive for ^{11}C-CH, whereas some low-grade gliomas may be negative for ^{11}C-CH.

11.2.1.3 Cell Proliferation

^{18}F-fluorothymidine (^{18}F-FLT) is a PET imaging agent commonly used to reflect the activity level of cell proliferation. ^{18}F-FLT is a thymidine analog that can be acted on by thymidine kinase I to enter cells and participate in metabolism, a process similar to the reaction between ^{18}F-FDG and hexokinase. However, unlike thymidine, ^{18}F-FLT has a low affinity for mitochondrial thymidine kinase II, and can therefore serve as a tracer that specifically targets the cell cycle. Therefore, ^{18}F-FLT PET can be used to quantify mitotic activity and cell division. Furthermore, since ^{18}F-FLT is only taken up by tumor cells in the S phase of the cell cycle, it has some level of specificity for the diagnosis of brain tumors. In terms of evaluating the efficacy of radiotherapy, the decrease in ^{18}F-FLT uptake value occurs earlier than that of ^{18}F-FDG, which implies that the former can be used to differentiate between radiation necrosis and tumor recurrence. Additionally, ^{18}F-FLT PET has shown superior accuracy and higher correlation with prognosis than ^{18}F-FDG PET for the diagnosis of recurrence in high-grade gliomas.

11.2.1.4 Others

Hypoxia is a key factor contributing to the progression and drug resistance of malignant tumors; therefore, the PET imaging of hypoxia occupies a crucial position in metabolic imaging, especially for post-radiotherapy brain tumors, and can serve as a non-invasive evaluation method. ^{18}F-fluoromisonidazole (^{18}F-FMISO) is currently the most commonly applied imaging agent for hypoxia. It can freely cross the blood-brain barrier and diffuse rapidly within tissues to attain equilibrium. This diffusion process is not affected by perfusion, and ^{18}F-FMISO will only be taken up by severely hypoxic cells. ^{18}F-FMISO PET images need to be calibrated using blood samples in order to calculate the tumor-to-blood ratio of ^{18}F-FMISO uptake, while a ratio of >1.2 indicates a higher ^{18}F-FMISO uptake in hypoxic tissues compared to normal tissues. This ratio can be combined with MRI anatomical images to delineate ROIs for the calculation of hypoxic tumor volume, which is an independent factor for determining the poor prognosis of malignant gliomas.

11.2.2 Applications of PET in Brain Tumors

PET imaging is able to reflect the biochemical, metabolic, and functional status of tumor tissues. There is a wide variety of intracranial tumors, about 90% of which can be localized and qualitatively diagnosed using CT and MRI, without the use of PET. In this section, we will focus on describing the application of PET imaging in gliomas, intracranial lymphomas, and brain metastases.

11.2.2.1 Glioma

Gliomas account for 40–50% of all intracranial tumors, while different grades of gliomas exhibit different levels of ^{18}F-FDG uptake. Some studies have shown that 86% of gliomas with decreased ^{18}F-FDG uptake are classified as grades I and II, whereas 94% of those with increased ^{18}F-FDG uptake are classified as grades III and IV (Fig. 11.11). Nevertheless, there are certain drawbacks to using ^{18}F-FDG PET imaging for the clinical classification of tumors. ^{18}F-FDG is a glucose analog that can directly reflect cellular energy metabolism. However, hexokinase II is overexpressed in some brain tumors, and its catalytic effect on ^{18}F-FDG entails that PET imaging may overestimate the glucose metabolic levels of these brain tumors to a certain extent, giving rise to false positive results. Examples of such tumors include pilocytic astrocytomas and gangliogliomas. Moreover, inflammation, active tuberculosis, granulation tissues, and certain benign tumors can also present high ^{18}F-FDG uptake. Additionally, owing to the relatively high glucose metabolism of the cerebral cortex, difficulties may arise in the accurate delineation of tumor boundaries and differentiation from surrounding normal tissues. In such cases, delayed ^{18}F-FDG imaging can be implemented, as it exploits the longer retention time of radioactive tracers in tumors compared to normal gray matter, thereby improving the discriminant ability between tumors and normal tissues. Another valuable contribution of ^{18}F-FDG PET imaging in brain tumors is the ability to discriminate between tumor recurrence and radiation necrosis. More
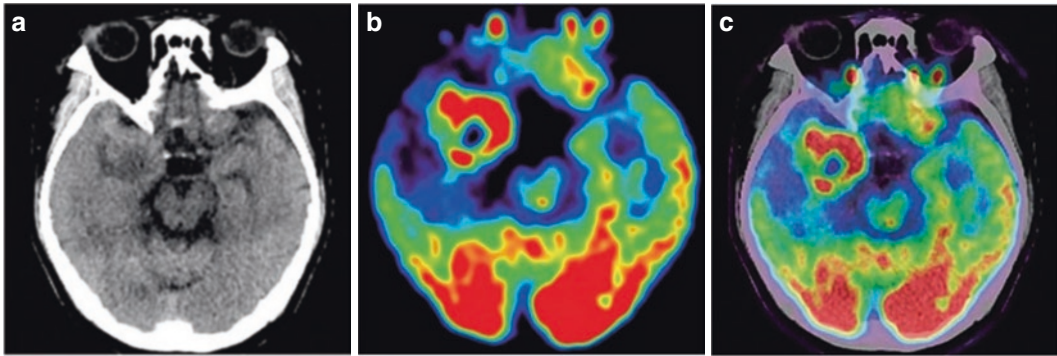
Fig. 11.11 High-grade glioma of the right temporal lobe. A 52-year-old male patient whose transverse brain CT shows a mass in the right temporal lobe, with a hypodense center and slightly hyperdense rim (**a**). Transverse ^{18}F-FDG PET (**b**) and integrated ^{18}F-FDG PET/CT (**c**) show significantly increased glucose metabolism at the rim, with a maximum standardized uptake value (SUV) of 5.75. Impaired glucose metabolism can be seen around the tumor, which signifies peritumoral edema

specifically, increased glucose uptake is observed in recurrent brain tumors, whereas decreased glucose metabolism is found in radiation necrosis. A recent meta-analysis reported that utilizing ^{18}F-FDG PET in the diagnosis of primary glioma recurrence gave an acceptable level of accuracy, with a diagnostic sensitivity of 0.77 [95% confidence interval (CI): 0.66–0.85] and specificity of 0.78 (95% CI: 0.54–0.91). Furthermore, this technique is suitable for gliomas of any histological type. However, occasionally in clinical practice, ^{18}F-FDG PET cannot clearly differentiate between tumor recurrence and radiotherapy-induced injury, regardless of whether gray or white matter is used as the reference standard. The main reason for this may be that normal brain tissue shows a relative increase in glucose uptake following radiotherapy, while the inflammatory changes caused by radiotherapy-induced injury also lead to varying degrees of increased FDG uptake.

[11]C-MET PET imaging of brain gliomas can produce positive results in more than 90% of cases, and significant ^{11}C-MET retention can be observed even in low-grade primary brain tumors, which are clearly demarcated from normal brain tissues. ^{11}C-MET can also be utilized in the identification and localization of malignant gliomas with a high risk of post-radiotherapy recurrence. A recent meta-analysis on the post-treatment recurrence of gliomas found that ^{11}C-MET PET showed a good accuracy for high-grade gliomas, with a sensitivity of 70% (95% CI: 50–84%) and specificity of 93% (95% CI: 44–100%).

^{18}F-FET is currently the most commonly used PET tracer for gliomas. There are overlaps in the levels of ^{18}F-FET uptake among different grades of gliomas. The tumor-to-brain ratio (TBR) derived from ^{18}F-FET PET can be used to differentiate between high- and low-grade gliomas with a sensitivity of 71–80% and a specificity of 56–85%, while the cutoff values of mean TBR and maximum TBR for the differentiation between high- and low-grade tumors are 1.9–2.9 and 2.5–2.7, respectively. A meta-analysis of 23 studies involving 994 patients showed that ^{18}F-FET PET had a significantly higher sensitivity than ^{18}F-FDG PET for the preoperative classification of gliomas (88 vs 63%), whereas ^{18}F-FDG PET had a higher specificity than ^{18}F-FET PET (89 vs 57%). In addition to providing information for the preoperative classification of gliomas, ^{18}F-FET PET can also supplement the prediction of glioma molecular subtypes (Figs. 11.12 and 11.13). Verger et al. divided 90 newly diagnosed, and untreated patients with gliomas into three groups: IDH-mutant and 1p/19q co-deleted oligodendrogliomas (16 cases), IDH-mutant astrocytomas (27 cases), and IDH-wildtype glioblastomas (47 cases). The results of their
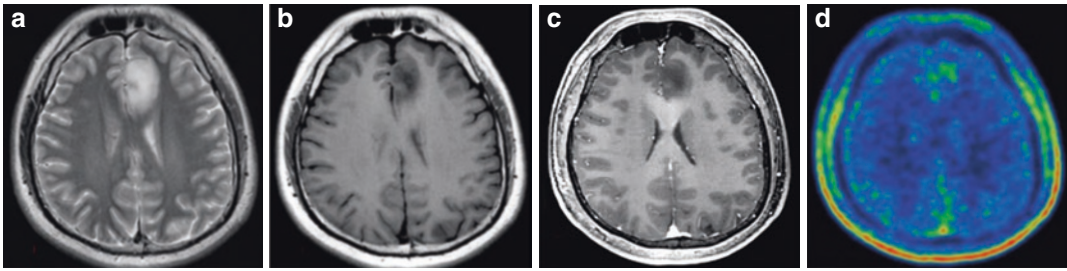
Fig. 11.12 Left frontal lobe oligodendroglioma, WHO grade II. A 19-year-old male patient whose MRI shows an oval mass in the left frontal lobe. Transverse T_2WI shows heterogeneous hyperintense signals (**a**); transverse T_1WI shows hypointense signals without significant edema (**b**); contrast-enhanced scan shows no significant enhancement (**c**); and transverse ^{18}F-FET PET shows slightly increased uptake within the lesion (**d**)
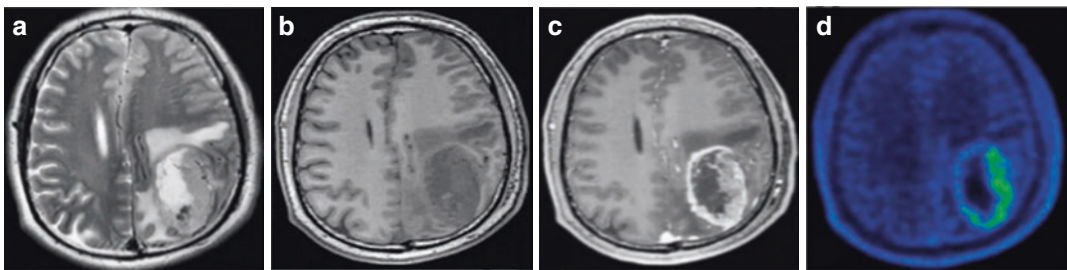
Fig. 11.13 Left parietal lobe glioblastoma, WHO grade IV. A 41-year-old male patient whose MRI shows an oval mass in the left parietal lobe. Transverse T_2WI shows heterogeneous mixed isointense and hyperintense signals (**a**); transverse T_1WI shows hypointense signals surrounded by finger-like edema signals (**b**); contrast-enhanced scan shows significant ring-like enhancement (**c**); and transverse ^{18}F-FET PET shows significantly increased uptake within the lesion (**d**)

study revealed that the mean TBR, maximum TBR, time-to-peak (TTP), and slope of ^{18}F-FET uptake could each discriminate between IDH-mutant astrocytomas and IDH-wildtype glioblastomas. Of these, mean TBR showed the best diagnostic performance, with an optimal cutoff value of 1.95, and a sensitivity, specificity, and accuracy of 89, 67, and 81%, respectively. Mean TBR, maximum TBR, TTP, and slope were all useful for predicting IDH mutation status, with the combined multiparametric prediction reaching an accuracy of up to 73%.

11.2.2.2 Intracranial Lymphoma

PCNSL is a rare malignant tumor of the CNS. It is classified as an invasive extranodal non-Hodgkin's lymphoma, and its pathological type is mostly diffuse large B-cell lymphoma. Despite its low incidence, PCNSL has a very high level of malignancy. Primary intracranial lymphomas generally do not involve the whole body and are mostly found in immunocompromised patients, such as patients with AIDS or patients receiving long-term immunosuppressive therapy after organ transplantation. PCNSL frequently occurs in the frontal lobe, temporal lobe, basal ganglia, corpus callosum, periventricular white matter, and cerebellum, either as single or multiple lesions. At present, the preliminary diagnosis of PCNSL depends primarily on CT and MRI. However, intracranial PCNSL shares many similar CT and MRI findings with other common intracranial space-occupying diseases (e.g., gliomas, and intracranial metastases of malignant tumors), which has led to a high rate of misdiagnosis. ^{18}F-FDG PET/CT is an imaging approach that integrates anatomical with functional information. It combines anatomical structural information with glucose metabolic status, in order to analyze the characteristics of lesions, which can
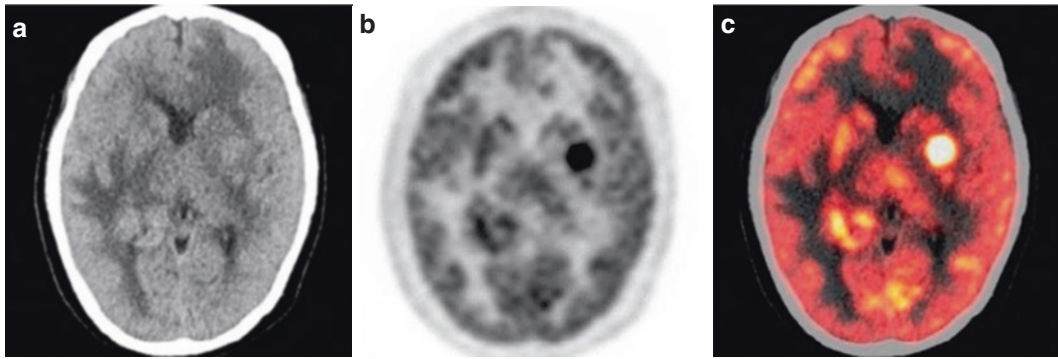
Fig. 11.14 Central nervous system lymphoma (diffuse large B-cell). A 68-year-old female patient whose transverse brain CT shows multiple hyperdense masses in the left basal ganglia, left frontal lobe, and right posterior horn of the lateral ventricle, surrounded by flaky hypoden- sities (**a**). Transverse ^{18}F-FDG PET (**b**) and integrated ^{18}F-FDG PET/CT (**c**) shows significant glucose hypermetabolism in the lesions above, showing a maximum standardized uptake value (SUV) of 10.49, and large areas of peripheral edema

facilitate the diagnosis of intracranial primary lymphomas. ^{18}F-FDG PET imaging of untreated intracranial lymphomas will reveal a clearly demarcated radioactive foci with a high level of retention (Fig. 11.14), but which still needs to be differentiated from single intracranial metastases. ^{18}F-FDG PET imaging can also be utilized in the evaluation of therapeutic efficacy in primary intracranial lymphomas. Additionally, ^{11}C-MET imaging can display clear radioactive foci, but the extent of these foci tends to be larger than that revealed in CT.

11.2.2.3 Brain Metastasis

MRI can be implemented to obtain a large amount of information related to brain metastases. Additionally, conventional structural imaging, MRI can also acquire functional metabolic information through diffusion, perfusion, and spectroscopic imaging. PET imaging is a useful supplement to MRI and can provide further metabolic information on brain metastases (Fig. 11.15). The principle of ^{18}F-FDG imaging for brain metastases is the same as that for primary intracranial tumors, which also implies it has a number of similar shortcomings in clinical application. For example, the high background noise in the cortex and basal ganglia can significantly reduce the signal-to-noise ratio of PET imaging, and its resolution is also relatively low, which has restricted its wider clinical applica-

tion. In addition to ^{18}F-FDG, other tracers, such as those reflecting the level of amino acid metabolism, can also be utilized in the diagnosis and efficacy evaluation of brain metastases. The active transport process of amino acid tracers can provide metabolic information without relying on impairments to the blood-brain barrier. Furthermore, the significantly lower background activity of amino acid tracers in the brain than ^{18}F-FDG is also another major advantage. However, neither ^{18}F-FDG nor amino acid PET imaging can accurately discriminate brain metastases from common primary malignant tumors of the brain, such as glioblastomas. Although ^{18}F-FET uptake may be higher in high-grade gliomas than low-grade gliomas, there are overlaps in the uptake values among glioblastomas, metastases, and inflammatory diseases such as multiple sclerosis. Even epileptogenic foci may cause abnormal ^{18}F-FET uptake. A large-scale study using ^{18}F-FET for the diagnosis of brain space-occupying lesions found no difference between the standardized uptake values (SUV) of high-grade gliomas and non-neoplastic lesions. Furthermore, ^{18}F-FET PET imaging showed a low sensitivity for micrometastases. Therefore, there has been an intensification in the research and development of novel PET tracers, with the aim of overcoming the limitations of PET imaging in clinical applications.
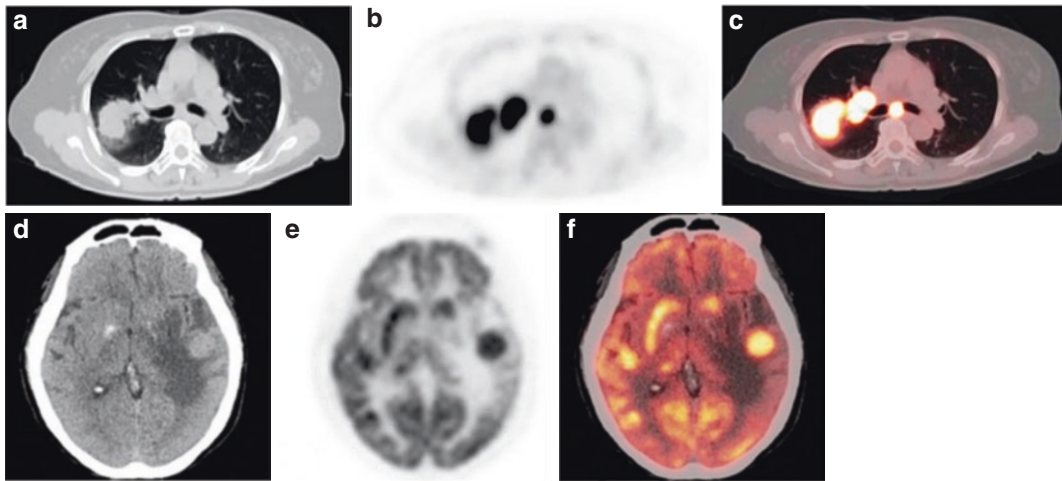
Fig. 11.15 Adenocarcinoma of the right upper lobe of the lung with mediastinal, right hilar, and brain metastases. A 70-year-old male patient. Transverse ^{18}F-FDG PET/CT shows soft tissue masses in the right upper lobe of the lung, with lobular and spiculate edges (**a**). Transverse ^{18}F-FDG PET (**b**) and integrated ^{18}F-FDG PET/CT (**c**) show significant glucose hypermetabolism of the lesion in the right lung, and right hilar and mediastinal metastatic lymph nodes. Transverse ^{18}F-FDG PET/CT shows hyperdense nodules in the left temporal lobe (**d**). Transverse ^{18}F-FDG PET (**e**) and integrated ^{18}F-FDG PET/CT (**f**) show significant glucose hypermetabolism of the lesions, with a large area of peripheral edema, suggestive of metastatic lesions

PET plays an important role in the formulation of treatment plans for brain metastases. A study reported on the use of MRI and ^{11}C-MET PET to evaluate the recurrence of brain metastasis treated with γ-knife radiosurgery. It was found that the irradiation field delineated based on ^{11}C-MET PET was smaller than that formulated under MRI guidance, but led to a longer patient survival time, suggesting that ^{11}C-MET PET can more effectively guide the delineation of the irradiation target. Similar findings were observed for ^{18}F-FET imaging. The increase in brain metastasis volume is not a marker of tumor progression. As with gliomas, radiation-induced changes may be mistaken for tumor progression; therefore, PET imaging can assist with the differentiation from radiation necrosis. In terms of ^{11}C-MET, its uptake in brain metastases is higher than that in radiation necrosis, with a sensitivity of 79% and specificity of 75%, while ^{18}F-FET uptake is significantly correlated with ^{11}C-MET uptake ($r = 0.84$). Furthermore, the results of dynamic ^{18}F-FET imaging showed that combining TBR (>1.9) with time-activity curves can achieve a diagnostic accuracy of up to 93%.

One of the current research hotspots is the discovery of early imaging-based markers for the evaluation of therapeutic efficacy, to improve the treatment strategies of patients. Therefore, there is a need to fully develop and validate imaging markers, whether they are based on MRI or PET, to fulfill their clinical applications.

11.3   Research Applications of PET/MR in Brain Tumors

Although MRI is a routine scan performed in brain tumors, conventional structural MRI may not be able to reliably predict the malignancy or growth potential of lesions. Furthermore, damage to normal brain structures caused by postoperative injury and chemoradiotherapy-induced necrosis, as well as non-specific treatment-induced signals such as inflammation, edema, demyelination, ischemia, and metal implants, have all increased the challenges faced by the clinical application of MRI. A number of new treatment strategies, such as anti-angiogenesis therapy or immunotherapy, may obscure or cause the enhancement of the affected area, which fur-

ther affects the diagnostic accuracy in the evaluation of post-treatment response. In patients with glioma receiving radiotherapy, the specificity of detecting glioma recurrence using conventional MRI may be as low as 50%. Among tumors with imaging features of low-grade gliomas characterized by the lack of enhancement, 40% of the final pathological confirmation may consist of high-grade components. fMRI, PET, and other functional imaging techniques can also reflect tissue-specific biological characteristics. Therefore, the combination of PET with MRI has potential implications for further improving overall diagnostic accuracy and patient management.

11.3.1 Advantages of Integrated PET/MR over Conventional Equipment

In recent years, a large number of studies have stressed on the potential application value of multiparametric integrated PET/MR in brain tumors. Preliminary studies have mainly focused on the practicality and consistency of multimodal imaging based on integrated PET/MR, and few have examined diagnostic accuracy. The earliest study on the accuracy of integrated PET/MR involved the comparison between PET/CT and PET/MR in evaluating the relationship of primary CNS tumors. The results revealed that the imaging quality of PET/MR and PET/CT both satisfied the diagnostic criteria, and the resulting TBR showed excellent concordance, with a Pearson's correlation coefficient of 0.98. Furthermore, compared to PET/CT, PET/MR had higher sensitivity and showed no artifacts or distortions in all images produced. Integrated PET/MR enables the simultaneous acquisition of PET and MRI, which allows the comparison of direction correlations among different imaging parameters obtained during a single scan session. This, in turn, helps us to explore the complementarity of metabolic or anatomical information provided by different modalities.

The preliminary investigations on PET/MR were mostly bimodal studies, mainly comparing the concordance and variability in the information obtained using either amino acid PET imaging or MRI alone. ^{18}F-FET PET imaging can display the malignancy and activity of gliomas, whereas PWI can reveal the microvascular proliferation and perfusion of tumor tissues. Filss et al. compared the differences between the imaging information provided by ^{18}F-FET PET and PWI in patients with brain tumors. A total of 56 patients with gliomas and 8 patients with meningiomas were enrolled in the study, for whom TBRs were calculated, while the tumor volumes, spatial congruence, and distance between local hot spots in ^{18}F-FET PET scans and PWI maps were assessed. Their results revealed that ^{18}F-FET PET could clearly discriminate between tumor tissues and normal regions, which was more difficult to accomplish using rCBV maps. Furthermore, in patients with gliomas, the TBR and tumor volumes based on ^{18}F-FET PET were significantly larger than in rCBV maps [TBR: 2.28 ± 0.99 vs. 1.62 ± 1.13, $P < 0.001$; tumor volume: (24.3 ± 26.5) cm^3 vs. (8.9 ± 13.9) cm^3; $P < 0.001$], while the spatial congruence between the two was poor, and the mean distance between local hot spots was (25.4 ± 16.1) mm. In patients with meningiomas, the TBR in ^{18}F-FET PET was significantly larger than in rCBV maps [TBR: $(5.33 \pm 2.63$ vs. 2.37 ± 0.32, $P < 0.001)$], but the spatial distribution of tumors was similar between the two. These findings imply that performing tumor imaging with ^{18}F-FET PET and rCBV in patients with gliomas can yield different information. Compared to rCBV maps, ^{18}F-FET PET showed significantly higher TBRs and tumor volumes, with a poor spatial congruence between the two parameters and a large variability in local hot spots. Taken together, the results indicate that rCBV as measured by PWI does not reflect the metabolically active tumor tissues of gliomas as depicted by amino acid PET. Apart from PWI, there is also an ongoing debate as to whether DWI indicators, such as minimum ADC, can be applied clinically in preoperative tumor classification and treatment planning. In order to establish the pathological correlate of minimum ADC, Rose et al. examined the relationship between minimum ADC and maximum ^{18}F-fluorodopa

(^{18}F-FDOPA) PET uptake in patients with newly diagnosed glioblastoma multiforme. In this study, MRI and ^{18}F-FDOPA PET data were acquired preoperatively from 15 patients with high-grade brain tumors (WHO grade III or IV), and regions of minimum ADC value within the tumor volume defined by ^{18}F-FDOPA PET was correlated with regions of maximum ^{18}F-FDOPA uptake. The results showed limited anatomical overlap between regions with minimum ADC and maximum TBR. Compared to the region with maximum ^{18}F-FDOPA TBR (2.45 ± 0.88) within the tumor tissues, the region with minimum ADC had a significantly lower ^{18}F-FDOPA TBR (1.36 ± 0.22, $P = 0.0001$). This implies that there is a poor correlation between minimum ADC and the most aggressive component of high-grade gliomas. Therefore, other factors, such as tissue compression or local ischemia, may have contributed to the restricted diffusion of glioblastomas. Therefore, caution should be exercised when utilizing minimum ADC as a marker of tumor grade and as a preoperative guidance for tumor biopsies in clinical practice.

11.3.2 Clinical Applications of Integrated PET/MR

### 11.3.2.1 Guidance for Preoperative Needle Biopsy

As the clinical application of PET/MR in brain tumors continues to advance, studies have found that this technique can provide useful guidance for the preoperative needle biopsy of brain tumors. Masada et al. reported the case of a 53-year-old male patient with malignant lymphoma who complained of walking and gait disturbances. MRI revealed multiple lesions of the bilateral frontal lobe, with significant enhancements in contrast-enhanced scan, while ^{18}F-FDG PET showed significant heterogeneous increases in lesion ^{18}F-FDG uptake. Needle biopsy was performed under the guidance of PET and MRI co-registration, and histological examination confirmed the lesion as malignant lymphoma, indicating that PET/MR co-registration can help to determine the most active component of brain

tumors. MRS and PET are both non-invasive imaging methods of proliferation-related cell metabolism and are therefore more likely to detect highly active tumor regions. Some researchers have attempted to incorporate preoperative MRS and PET into the intraoperative navigation system to guide the surgical biopsy and tumor sampling of gliomas, thereby improving the intraoperative characterization of tumor tissues and verification of imaging biomarkers. Their results demonstrated that this approach enabled neurosurgeons to sample the tumor region based on physiological and molecular imaging markers. In a case of needle biopsy performed within a pathologically confirmed astrocytoma (WHO grade II), a region without marked enhancement but with elevated local Cho peak and increased ^{11}C-MET uptake was confirmed through needle biopsy as an early malignant transformation zone. MRI is the most common method utilized to determine the location and extent of gliomas. In a prospective study, Pauleit et al. explored whether diagnostic accuracy could be improved by combining MRI with ^{18}F-FET PET. Co-registration was performed between the ^{18}F-FET PET and MRI images of 31 patients with suspected gliomas, followed by needle biopsies at regions with both abnormal MRI signals and increased ^{18}F-FET uptake (match), as well as regions with abnormal MRI signals but normal ^{18}F-FET uptake or vice versa (mismatch), which gave a total of 52 biopsy samples. The results showed that the diagnostic performance (as measured using AUC) of needle biopsies based on MRI alone was 0.80, with a sensitivity of 96% for detecting tumor tissues, and a specificity of only 53%; whereas the diagnostic performance of MRI combined with ^{18}F-FET PET increased to 0.98, with a sensitivity of 93% and specificity of 94%. These findings indicate that the combined use of MRI and ^{18}F-FET PET in patients with gliomas significantly improves the identification of glioma tissues, which has significant implications for target selection in the diagnostic biopsies and treatment planning of gliomas.

Several studies have demonstrated that amino acid PET imaging shows a different glioma extent from conventional plain and contrast-

enhanced MRI (Fig. 11.16), while the combination of the two can help to guide the extent of surgical resection and determine the target area of radiotherapy. In a study on 50 patients with newly diagnosed, untreated glioblastoma, Lohmann et al. performed a retrospective analysis on the tumor volumes delineated by ^{18}F-FET PET (V_{PET}) and by contrast-enhanced and FLAIR MRI (V_{MRI}). They found that 43 patients (86%) showed significantly larger V_{PET} than V_{MRI} [(21.5 ± 14.3) mL vs. (9.4 ± 11.3) mL; $P < 0.001$], while 40 patients (80%) showed both increased FET uptake and significant contrast enhancement, but with low spatial similarity in tumor volume between the two, and 10% of patients showing increased ^{18}F-FET uptake beyond the areas of abnormal FLAIR signals. Taken together, this study has shown that the tumor volume delineated by ^{18}F-FET PET is significantly larger than that by MRI contrast enhancement, which

strongly suggests that the information derived from the two modalities should be combined to guide the treatment and diagnosis of patients with newly diagnosed glioblastomas. Some researchers argue that contrast-enhanced MRI cannot reflect the entire infiltration extent of gliomas, whereas the amino acid tracer, ^{18}F-DOPA, shows a higher TBR and sensitivity for gliomas. Therefore, they compared between the tumor extents delineated by PET and conventional MRI in 10 patients with glioma and obtained 23 biopsy samples from matched or mismatched areas between metabolism and contrast enhancement. Their findings revealed that among the 16 samples histopathologically confirmed as high-grade gliomas, 13 were obtained from areas with increased metabolism, whereas only 6 were obtained from areas with contrast enhancement in contrast-enhanced images. Given these results, they concluded that ^{18}F-DOPA PET metabolism
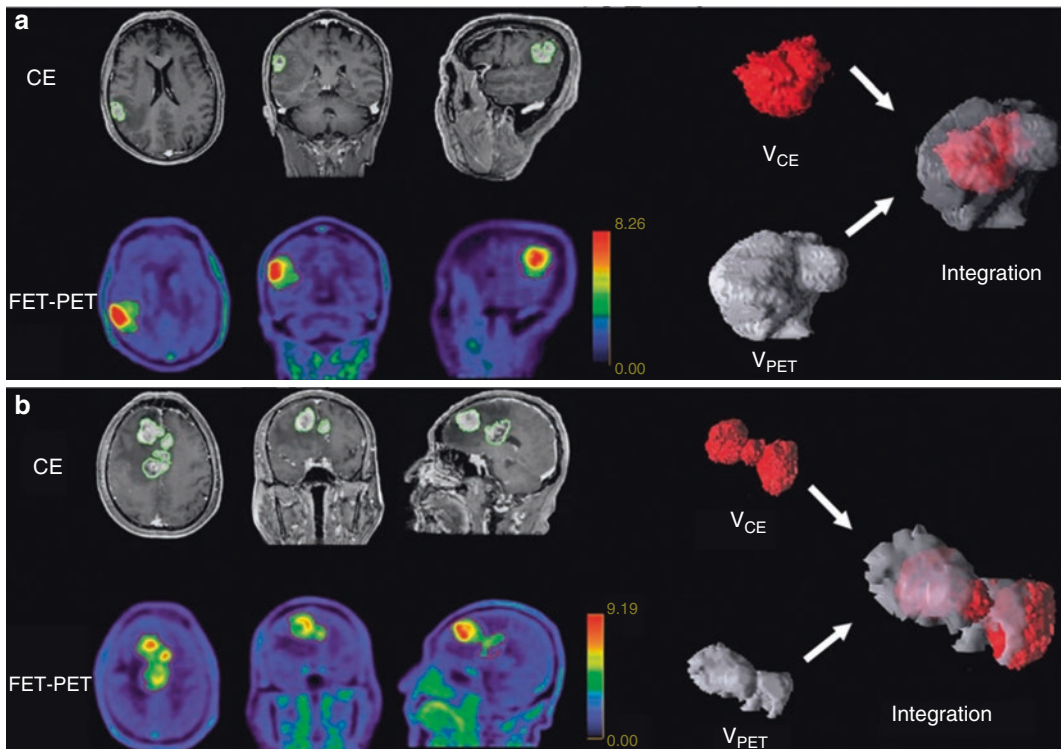
Fig. 11.16 Integrated ^{18}F-FET PET/MR improves the presentation of glioma spatial distribution. ^{18}F-FET-PET and contrast-enhanced (CE) MRI show low spatial similarity but large overlaps. V_{PET} is significantly larger than V_{CE}, and most of V_{CE} is contained within V_{PET} (**a**). There is high spatial dissimilarity between V_{PET} and V_{CE} (**b**), and the two are mutually complementary in the delineation of the entire tumor. Arrows: integration

can more accurately identify higher-grade regions within gliomas, and is therefore valuable in guiding the target selection of stereotactic biopsies.

### 11.3.2.2 Assistance for Preoperative Diagnosis of Brain Tumors

PET/MR is also valuable for the preoperative diagnosis of brain tumors. Findings on the use of MRI features alone to discriminate between high- and low-grade gliomas have remained controversial. In view of this, a retrospective analysis was performed on 127 patients with MRI-suspected low-grade gliomas, who were enrolled based on the following inclusion criteria: lesions with no significant contrast enhancement, showing hyperintense T_2WI signals, hypointense T_1WI signals, and no intralesional hemorrhage or necrosis. The final pathological confirmation revealed that 47 patients had high-grade glioma, and 7 had non-neoplastic lesions; 97 patients exhibited ^{18}F-FET hypermetabolism, of whom 93 patients with neoplastic lesions, 69% with low-grade gliomas, and 89% with high-grade gliomas showed increased ^{18}F-FET uptake; the kinetic analysis of ^{18}F-FET showed that the sensitivity for high-grade gliomas was 95%; specificity, 72%; positive predictive value, 74%; and negative predictive value, 95%. Based on these findings, it can be seen that among MRI-suspected low-grade gliomas, the kinetic analysis of ^{18}F-FET showed an extremely high sensitivity for the detection of high-grade gliomas. Given that PWI and ^{18}F-FET PET can both provide grading information for gliomas, researchers have compared the diagnostic value of ^{18}F-FET PET and PWI for the tumor grading of patients with newly diagnosed, untreated gliomas using an integrated PET/MR scanner. They found that both techniques showed high accuracy in the discrimination of high- and low-grade gliomas. In order to further elucidate the value of molecular imaging for exploring intratumoral heterogeneity in low-grade gliomas, Kunz et al. designed a prospective study involving 55 patients with MRI-suspected WHO grade II gliomas. By analyzing the kinetic curve characteristics of ^{18}F-FET, the patients were divided into three subgroups: (1) a homogeneous WHO grade II glioma group (30 patients), (2) a homogeneous malignant glioma group (10

patients), and (3) a heterogeneous group exhibiting both low- and high-grade characteristics at different sites (15 cases). The assessment of 373 biopsy samples obtained from these patients revealed a strong correlation between tumor grade and uptake kinetics ($P < 0.0001$). Homogeneous patterns of uptake kinetics were associated with homogeneous histopathological findings, while heterogeneous patterns were associated with histopathological heterogeneity. Furthermore, local hot spots exhibiting characteristics of malignant glioma accounted for 4–44% of the entire tumor volume; therefore, the researchers concluded that in MRI-suspected WHO grade II gliomas, ^{18}F-FET uptake kinetics were closely linked with intratumoral histopathology, which can facilitate the accurate identification of local anaplastic foci and has significant implications for prognostic evaluation and treatment planning. Haubold et al. utilized radiomics to analyze the value of multiparametric ^{18}F-FET PET/MR in guiding the preoperative grading and genotype prediction of 42 patients with gliomas. They found that the combination of contrast-enhanced MRI, ^{18}F-FET PET, and SWI showed the best performance in discriminating between high- and low-grade gliomas, with an AUC, sensitivity, and specificity of 0.85, 83.1%, and 79.6%, respectively; the AUC and sensitivity were lower than those of this study. Moreover, the AUCs of this combination in predicting glioma IDH1 mutation, 1p/19q co-deletion, and MGMT promoter methylation status were 0.887, 0.978, and 0.757, respectively. Another study found that multimodal imaging using integrated ^{18}F-FET PET/MR allows the non-invasive prediction of glioma IDH mutation status, and the discrimination of IDH-wildtype glioblastomas (Fig. 11.17) from IDH-mutant astrocytomas without 1p/19q co-deletion (Fig. 11.18), providing imaging evidence for the accurate preoperative diagnosis of gliomas, guidance of clinical treatment decisions, and evaluation of patient prognosis. However, this technique had limited value in discriminating between IDH-mutant, 1p/19q co-deleted oligodendrogliomas and IDH-mutant astrocytomas without 1p/19q co-deletion (Fig. 11.19), and therefore requires further investigation.
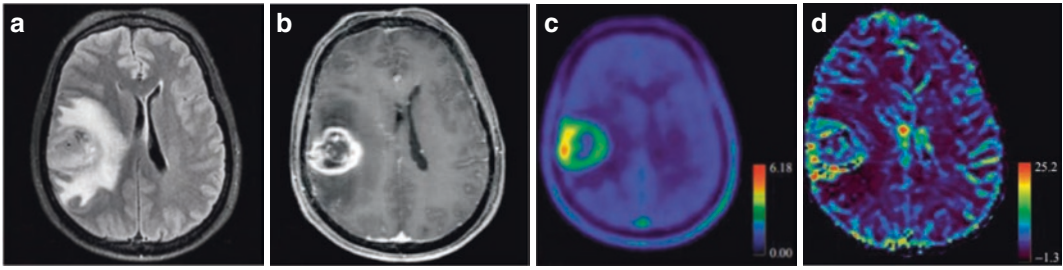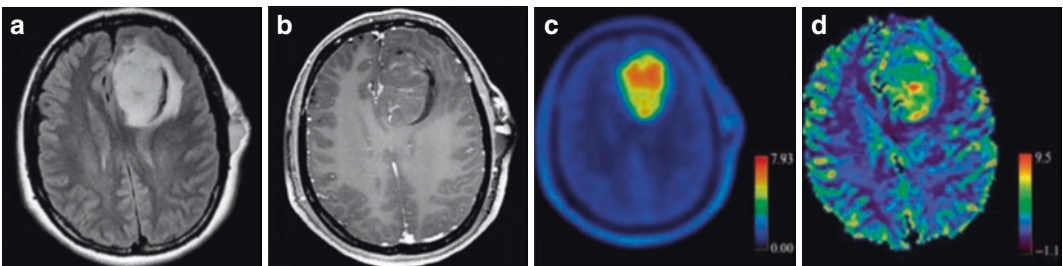
Fig. 11.17 IDH-wildtype glioblastoma, WHO grade IV. A 53-year-old male patient, whose integrated PET/MR shows a round mass in the right parietal lobe. Transverse FLAIR shows heterogeneous mixed hyper- and hypointense signals with finger-like perilesional edema (**a**); contrast-enhanced scan shows a heterogeneous ring-enhancing lesion (**b**); transverse ^{18}F-FET PET shows significantly enhanced uptake within the lesion, with TBR_{mean} and TBR_{max} values of 2.48 and 4.83, respectively (**c**); and the solid component of the lesion shows significantly elevated CBV, with relative mean and maximum CBV values of 2.78 and 6.63, respectively (**d**)
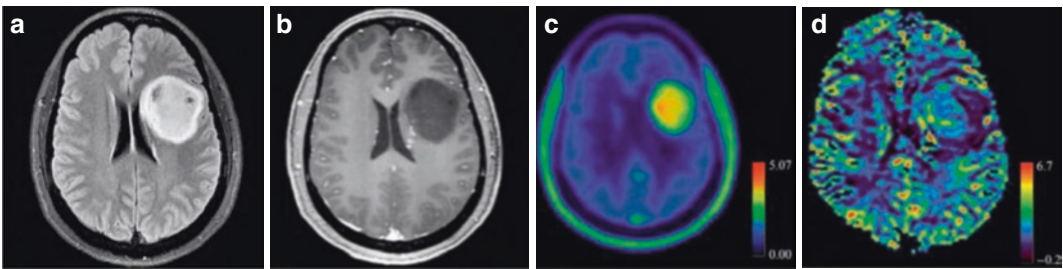
Fig. 11.18 IDH-mutant astrocytoma without 1p/19q co-deletion. A 31-year-old female patient, whose integrated PE/MRI shows a round mass in the left frontoparietal lobe. Transverse FLAIR shows heterogeneous hyperintense signals without significant perilesional edema (**a**); contrast-enhanced scan shows no significant contrast enhancement (**b**); transverse ^{18}F-FET PET shows significantly enhanced uptake within the lesion, with TBR_{mean} and TBR_{max} values of 2.35 and 3.74, respectively, which are both lower than those of IDH-wildtype glioblastoma and IDH-mutant, 1p/19q co-deleted oligodendroglioma (**c**); and lesion CBV is slightly elevated compared to the contralateral side, with relative mean and maximum CBV values of 0.83 and 3.24, respectively, which are both lower than those of IDH-wildtype glioblastoma and IDH-mutant, 1p/19q co-deleted oligodendroglioma (**d**)


Fig. 11.19 IDH-mutant, 1p/19q co-deleted oligodendroglioma, WHO grade III. A 34-year-old female patient, whose integrated PET/MR shows a round mass in the left frontal lobe. Transverse FLAIR shows heterogeneous hyperintense signals with patchy perilesional edema (**a**); contrast-enhanced scan shows mild punctate enhancement within the lesion (**b**); transverse ^{18}F-FET PET shows significantly enhanced uptake within the lesion, with TBR_{mean} and TBR_{max} values of 3.98 and 7.35, respectively (**c**); and lesion CBV is significantly elevated, with relative mean and maximum CBV values of 1.08 and 3.33, respectively (**d**)

11.3.2.3 Evaluation of Therapeutic Efficacy and Prognosis in Brain Tumors

PET/MR is an important approach in the follow-up and evaluation of therapeutic efficacy in the treatment of brain tumors (Fig. 11.20), discrimination between true recurrence and pseudo-progression, and prognostic prediction. In a study involving 16 patients with glioma undergoing standard radiotherapy, preoperative ^{18}F-FET PET/CT, and ^{18}F-FET PET/MR (including DWI, PWI, etc.) were performed, and the correlation between multimodal imaging parameters and tumor recurrence was analyzed. The results of the study indicated that performing multiparametric imaging before radiotherapy was feasible, and significant parametric differences were observed between the recurring and non-recurring groups at the voxel level. Furthermore, combining the imaging parameters is a logistic regression model allowed the prediction of recurrence probability in glioma patients, in which ^{18}F-FET was found to be the most important predictor. Quantitative volumetric (3D-VOI) lesion analysis has also been utilized to examine the diagnostic potential of integrated ^{18}F-FET PET/MR for the differentiation between recurrent gliomas and post-treatment-related effects (PTRE). In this retrospective study, recurrence was evaluated in 42 patients, including 32 patients with histologically confirmed glioma recurrence and 10 patients with PTRE, for whom, the mean (relative) ADC (ADC_{mean}, $rADC_{mean}$) and TBR were calculated. The results indicated that the glioma recurrence group showed higher ADC_{mean} and TBR_{max} than the PTRE group ($P < 0.05$). Both ADC_{mean} and TBR_{max} demonstrated reliable diagnostic performance in differentiating between glioma recurrence and PTRE. Furthermore, the bivariate analysis based on ADC_{mean} and TBR_{max} showed the highest diagnostic accuracy of up to 90% and is therefore useful for providing clinical guidance.
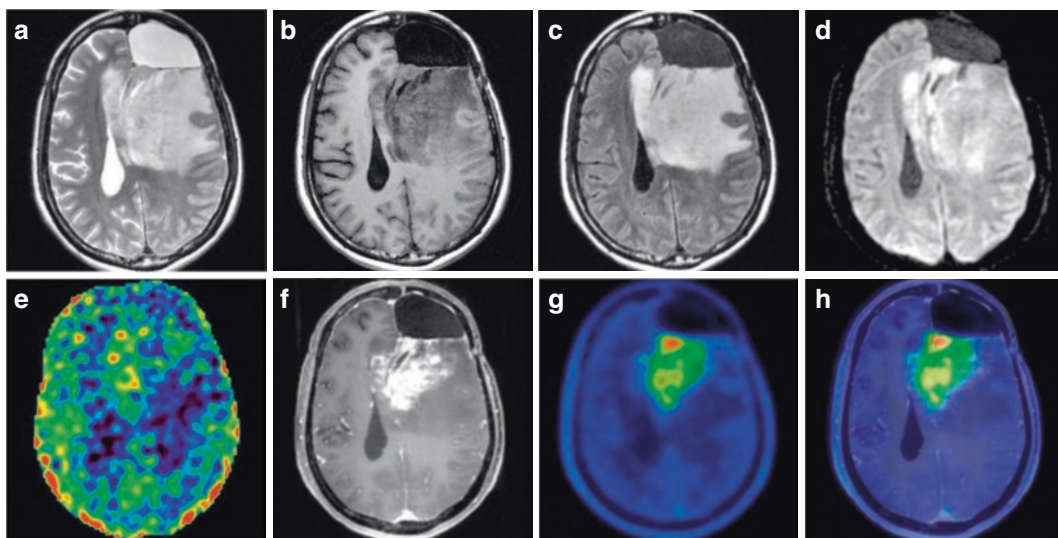
Fig. 11.20 Diagnosis of postoperative glioma recurrence using integrated ^{18}F-FET PET/MR. Integrated PET/MR shows an irregular mass in the left frontoparietal lobe, as well as a residual postoperative cavity situated anterior to the lesion. Transverse T_2WI shows heterogeneous hyperintense signals (**a**); transverse T_1WI shows heterogeneous hypointense signals (**b**); transverse FLAIR shows heterogeneous hyperintense signals with a small amount of perilesional edema (**c**); transverse DWI shows heterogeneous hyperintense signals (**d**); transverse ASL shows heterogeneous increases in lesion CBF (**e**); contrast-enhanced scan shows significant contrast enhancement (**f**); transverse ^{18}F-FET PET shows significant heterogeneous increased uptake within the lesion (**g**, **h**)

In summary, the clinical applications of combining PET and MRI are extremely valuable in neuro-oncology. Regardless of using separate scans that are subsequently merged, or one-stop scanning using integrated PET/MR, the use of such techniques will increase over the next few years. Although exciting results have been achieved through the combination of amino acid PET and advanced MRI techniques, more research is needed to determine its best applications. Integrated PET/MR scanners are expected to improve patient comfort and their potential as a one-stop imaging technique in neuro-oncology will be fully realized in the future.

Suggested Reading

Wang LL, Leach JL, Breneman JC, et al. Critical role of imaging in the neurosurgical and radiotherapeutic management of brain tumors. Radiographics. 2014;34(3):702–21.

Leu K, Ott GA, Lai A, et al. Perfusion and diffusion MRI signatures in histologic and genetic subtypes of WHO grade II-III diffuse gliomas. J Neurooncol. 2017;134(1):177–88.

Barajas RFJR, Rubenstein JL, Chang JS, et al. Diffusion-weighted MR imaging derived apparent diffusion coefficient is predictive of clinical outcome in primary central nervous system lymphoma. AJNR Am J Neuroradiol. 2010;31(1):60–6.

Huang WY, Wen JB, Wu G, et al. Diffusion-Weighted Imaging for Predicting and Monitoring Primary Central Nervous System Lymphoma Treatment Response. AJNR Am J Neuroradiol. 2016;37(11):2010–8.

Farquharson S, Tournier JD, Calamante F, et al. White matter fiber tractography: why we need to move beyond DTI. J Neurosurg. 2013;118(6):1367–77.

Delgado AF, Delgado AF. Discrimination between Glioma Grades II and III Using Dynamic Susceptibility Perfusion MRI: A Meta-Analysis. Am J Neuroradiol. 2017;38(7):1348–55.

Morabito R, Alafaci C, Pergolizzi S, et al. DCE and DSC perfusion MRI diagnostic accuracy in the follow-up of primary and metastatic intra-axial brain tumors treated by radiosurgery with cyberknife. Radiat Oncol. 2019;14(1):65.

Nakamura H, Doi M, Suzuki T, et al. The Significance of Lactate and Lipid Peaks for Predicting Primary Neuroepithelial Tumor Grade with Proton MR Spectroscopy. Magn Reson Med Sci. 2018;17(3):238–43.

Dimou S, Battisti RA, Hermens DF, et al. A systematic review of functional magnetic resonance imaging and diffusion tensor imaging modalities used in presur-gical planning of brain tumour resection. Neurosurg Rev. 2013;36(2):205–14.

Zulfiqar M, Dumrongpisutikul N, Intrapiromkul J, et al. Detection of intratumoral calcification in oligodendrogliomas by susceptibility-weighted MR imaging. Am J Neuroradiol. 2012;33(5):858–64.

Zhang L, Min Z, Tang M, et al. The utility of diffusion MRI with quantitative ADC measurements for differentiating high-grade from low-grade cerebral gliomas: evidence from a meta-analysis. J Neurol Sci. 2017;373:9–15.

Chen Z, Tie Y, Olubiyi O, et al. Reconstruction of the arcuate fasciculus for surgical planning in the setting of peritumoral edema using two-tensor unscented Kalman filter tractography. Neuroimage Clin. 2015;7:815–22.

Chen W, Cloughesy T, Kamdar N, et al. Imaging proliferation in brain tumors with 18F-FLT PET: comparison with ^{18}F-FDG. J Nucl Med. 2005;46(6):945–52.

Spence AM, Muzi M, Mankoff DA, et al. ^{18}F-FDG PET of gliomas at delayed intervals: improved distinction between tumor and normal gray matter. J Nucl Med. 2004;45(10):1653–9.

Nihashi T, Dahabreh IJ, Terasawa T. Diagnostic accuracy of PET for recurrent glioma diagnosis, a meta-analysis. Am J Neuroradiol. 2013;34(5):944–50.

Hutterer M, Nowosielski M, Putzer D, et al. [^{18}F]-fluoro-ethyl-L-tyrosine PET: a valuable diagnostic tool in neuro-oncology, but not all that glitters is glioma. Neuro Oncol. 2013;15(5):341–51.

Unterrainer M, Galldiks N, Suchorska B, et al. ^{18}F-FET PET uptake characteristics in patients with newly diagnosed and untreated brain metastasis. J Nucl Med. 2017;58(4):584–9.

Momose T, Nariai T, Kawabe T, et al. Clinical benefit of ^{11}C-methionine PET imaging as a planning modality for radiosurgery of previously irradiated recurrent brain metastases. Clin Nucl Med. 2014;39(11):939–43.

Grosu AL, Astner ST, Riedel E, et al. An interindividual comparison of O-(2[18F]fluoroethyl)-L-tyrosine(FET)-and L-[methyl-11C] methionine(MET)-PET in patients with brain gliomas and metastases. Int J Radiat Oncol Biol Phys. 2011;81(4):1049–58.

Ceccon G, Lohmann P, Stoffels G, et al. Dynamic O-(2-18F-fluoroethyl)-L-tyrosine positron emission tomography differentiates brain metastasis recurrence from radiation injury after radiotherapy. Neuro Oncol. 2016;19(2):281–8.

Jansen N, Graute V, Armbruster L, et al. MRI-suspected low-grade glioma: is there a need to perform dynamic FET PET? Eur J Nucl Med Mol Imaging. 2012;39(6):1021–9.

Kunz M, Thon N, Eigenbrod S, et al. Hot spots in dynamic(FET)-F-18-PET delineate malignant tumor parts within suspected WHO grade II gliomas. Neuro Oncol. 2011;13(3):307–16.

Galldiks N, Langen K, Pope WB. From the clinician's point of view-What is the status quo of positron emis-

sion tomography in patients with brain tumors? Neuro Oncol. 2015;17(11):1434–44.

Albert NL, Weller M, Suchorska B, et al. Response Assessment in Neuro-Oncology working group and European Association for Neuro-Oncology recommendations for the clinical use of PET imaging in gliomas. Neuro Oncol. 2016;18(9):1199–208.

Fink JR, Muzi M, Peck M, et al. Multimodality brain tumor imaging: MR imaging, PET, and PET/MR imaging. J Nucl Med. 2015;56(10):1554–61.

Catana C, Drzezga A, Heiss W, et al. PET/MRI for neurologic applications. J Nucl Med. 2012;53(12):1916–25.

Werner P, Barthel H, Drzezga A, et al. Current status and future role of brain PET/ MRI in clinical and research settings. Eur J Nucl Med Mol Imaging. 2015;42(3):512–26.

Filss CP, Galldiks N, Stoffels G, et al. Comparison of ^{18}F-FET PET and perfusion-weighted MR imaging: a PET/MR imaging hybrid study in patients with brain tumors. J Nucl Med. 2014;55(4):540–5.

Rose S, Fay M, Thomas P, et al. Correlation of MRI-derived apparent diffusion coefficients in newly diagnosed gliomas with [18F]-Fluoro-L-Dopa PET: what are we really measuring with minimum ADC? Am J Neuroradiol. 2013;34(4):758–64.

Pauleit D, Floeth F, Hamacher K, et al. O-(2-[18F]fluoroethyl)-L-tyrosine PET combined with MRI improves the diagnostic assessment of cerebral gliomas. Brain. 2005;128(3):678–87.

Song S, Cheng Y, Ma J, et al. Simultaneous FET-PET and contrast-enhanced MRI based on hybrid PET/MR improves delineation of tumor spatial biodistribution in gliomas: a biopsy validation study. Eur J Nucl Mol Imaging. 2020;47(6):1458–67.

Lohmann P, Stavrinou P, Lipke K, et al. FET PET reveals considerable spatial differences in tumour burden compared to conventional MRI in newly diagnosed glioblastoma. Eur J Nucl Med Mol Imaging. 2019;46(3):591–602.

Pafundi DH, Laack NN, Youland RS, et al. Biopsy validation of F-18DOPA PET and biodistribution in gliomas for neurosurgical planning and radiotherapy target delineation: results of a prospective pilot study. Neuro Oncol. 2013;15(8):1058–67.

Verger A, Filss CP, Lohmann P, et al. Comparison of ^{18}F-FET PET and perfusion-weighted MRI for glioma grading: a hybrid PET/MR study. Eur J Nucl Med Mol Imaging. 2017;44(13):2257–65.

Jena A, Taneja S, Gambhir A, et al. Glioma Recurrence Versus Radiation Necrosis: Single-Session Multiparametric Approach Using Simultaneous O-(2-18F-Fluoroethyl)L-Tyrosine PET/MRI. Clin Nucl Med. 2016;41(5):e228–36.

Jena A, Taneja S, Jha A, et al. Multiparametric evaluation in differentiating glioma recurrence from treatment-induced necrosis using simultaneous ^{18}F-FDG-PET/MRI: a single-institution retrospective study. Am J Neuroradiol. 2017;38(5):899–907.

Tomura N, Kokubun M, Saginoya T, et al. Differentiation between treatment-induced necrosis and recurrent tumors in patients with metastatic brain tumors: comparison among ^{11}C-Methionine-PET, FDG-PET, MR permeability imaging, and MRI-ADC–preliminary results. Am J Neuroradiol. 2017;38(8):1520–7.

Lundemann M, Munck AF, Rosenschöld P, et al. Feasibility of multi-parametric PET and MRI for prediction of tumour recurrence in patients with glioblastoma. Eur J Nucl Med Mol Imaging. 2019;46(3):603–13.